Transition metal oxides as electrocatalysts for the oxygen evolution reaction in alkaline solutions: An application-inspired renaissance

Fang Song,[1] Lichen Bai,[1] Aliki Moysiadou,[1] Seunghwa Lee,[1] Chao Hu,[1,2] Laurent Liardet,[1] and Xile Hu*,[1]

[1]Laboratory of Inorganic Synthesis and Catalysis, Institute of Chemical Sciences and Engineering, Ecole Polytechnique Fédérale de Lausanne (EPFL), EPFL-ISIC-LSCI, BCH 3305, Lausanne, CH 1015 Switzerland.

[2]School of Chemical Engineering and Technology, Xi'an Jiaotong University, Xi'an 710049, China.

ABSTRACT: Water splitting is the essential chemical reaction to enable the storage of intermittent energies such as solar and wind in the form of hydrogen fuel. The oxygen evolution reaction (OER) is often considered as the bottleneck in water splitting. While metal oxides had been reported as OER electrocatalysts more than half a century ago, the recent interest in renewable energy storage has spurred a renaissance of the studies of transition metal oxides as Earth-abundant and non-precious OER catalysts. This perspective presents major progress in several key areas of the field such as theoretical understanding, activity trend, in situ and operando characterization, active site determination, and novel materials. A personal overview of the past achievements and future challenges is also provided.

1. Introduction

Exploiting safe, clean, and sustainable energy sources is a major societal and technological challenge in the 21st century.[1-3] Solar, and to a less degree, wind energy, are in principle able to meet a large portion of the global energy demand. However, they are intermittent and require efficient and economic storage solutions. Among various storage solutions,[2] the water splitting reaction ($2H_2O \rightarrow O_2 + 2H_2$) is an attractive solution as it enables the sustainable production of hydrogen, a desirable energy carrier.[2,4,5] Water splitting can be divided into two half reactions, the hydrogen evolution reaction (HER, $2H^+ + 2e^- \rightarrow H_2$) and the oxygen evolution reaction (OER, $2H_2O \rightarrow O_2 + 4H^+ + 4e^-$). Both reactions are kinetically sluggish, and even with the best available catalysts, they require an overpotential (η) to occur at a useful rate. The overpotential loss due to OER is generally much greater than the loss due to HER. Thus, OER is often regarded as the bottleneck of water splitting.[4-7] Efficient, stable, abundant, and cost-effective OER catalysts are required to make water splitting a viable and scalable energy storage technology.

RuO_2 and IrO_2 had been considered as the benchmarks of OER catalysts because they exhibited high activity at a wide range of pH values.[8] For a reference current density (j) of 10 mA cm^{-2}, an overpotential of 200 mV (in acid) to 300 mV (in base) is required for thin films of RuO_2 and IrO_2. While these catalysts are employed in proton exchange membrane water electrolyzers, they might be too scarce and costly for a large-scale application.

The technological need of OER catalysts has motivated intense research efforts on the development of catalysts that are solely composed of Earth-abundant elements.[4,6,7,9-12] These catalysts might be classified into two categories: homogeneous, molecular complexes and heterogeneous, inorganic solids.[10,11] Molecular catalysts[13] have uniform and easy-to-identify active sites; they are readily characterized by spectroscopy and X-ray crystallography. Their properties can be finely turned by ligand modification. The mechanistic understanding of molecular OER catalysis is more advanced than its heterogeneous counterparts. Notwithstanding these desirable features, molecular catalysts suffer from their low long-term stability under the harsh conditions of OER and the difficulty to integrate them into electrochemical and photoelectrochemical devices. In this regard, heterogeneous inorganic catalysts are more practical. They often exhibit notable stability at OER potentials. Many of them have been deposited onto electrodes to catalyze OER with significant current densities (> 1 mA cm^{-2}) at modest overpotentials (300-400 mV).

Commercial electrolyzers operate in highly conductive medium, that is, either in acidic or alkaline conditions. Unfortunately, only RuO_x, IrO_x, and their composites exhibit substantial stability in acidic medium, where the majority of non-precious metal oxide OER catalysts gradually or rapidly degrade. Thus, non-precious metal oxide OER catalysts are mostly studied in alkaline medium. Scholarly studies of Co-, Ni-, Fe- and Mn-based oxides or hydroxides in OER dated back to more than half a century ago.[14-19] The samples used in these early studies were either bulk oxides or electrochemically deposited films. Sample purity and structural homogeneity were not strictly controlled. The characterization was largely limited to electrochemical measurements. As a result, mostly phenomenal findings were reported and the field progressed slowly. Several important technological advances make the timing ripe for the recent renaissance. Thanks to developments in nanoscience and nanotechnology, it is now possible to synthesize a wide range of metal oxides with controlled composition, morphology, size, structure, and surface areas. Modern analytical tools in spectroscopy and microscopy, especially the access to in situ and operando techniques, provide unprecedented fundamental information about the catalytic sites. Progress in density functional theory (DFT) computations makes it possible to calculate

the properties and even catalytic activity of metal oxides with a reasonable accuracy.

The recent developments of transition metal oxide catalysts for OER in alkaline solution have been described in a number of reviews.[4,6,7,10-12,20] These reviews tend to be comprehensive and are geared towards specialists. Here we select representative studies to offer our perspective of the key progress, debate, and challenge in this field. In addition to providing a critical selection of current studies for active researchers in the field, this perspective aims to give a bird's eye view for non-specialists who wish to enter the field.

2. Reaction mechanism

A general mechanism of OER on metal oxides in alkaline medium is described in **Figure 1**.[4,11,21] Here the active site is simply drawn as "M". In the first step, a hydroxyl radical is adsorbed on the active site to give M-OH by 1 e oxidation of hydroxide anion. Coupled proton and electron removals from M-OH then gives M-O. In one pathway, nucleophilic attack of hydroxyl anion on M-O coupled with 1 e oxidation yields the hydroperoxide intermediate M-OOH. A further proton-coupled electron transfer resulted in the release of O_2 and the regeneration of the free active site. In another pathway, combination of two M-O species gives directly O_2 and M. The mechanism depicted here forms the blueprint for the majority of proposed mechanisms, with the main variation being the number of electron or proton transfer in individual steps. In some cases, proton and electron transfers are proposed to be decoupled.[22]
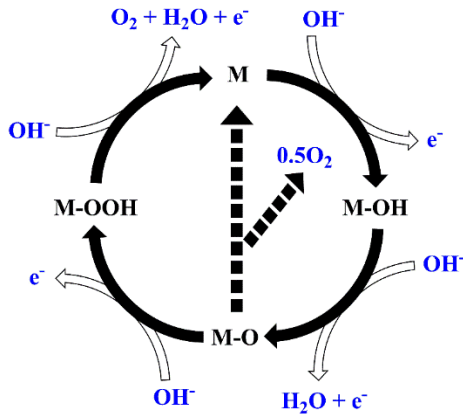

Figure 1. A generalized OER mechanism. M represents the active site.

The relationship of current density (j) and overpotential (η) in an electrochemical reaction can be described by the Butler-Volmer equation (Eq. 1). Here j_0 is the exchange current density, n is the number of transferred electrons, F is the Faraday's constant, R is the universal gas constant, T is the thermodynamic temperature, α_a and α_c is the transfer coefficient of anodic reaction and cathodic reaction, respectively. α_a and α_c are normally assumed to be 0.5. When the anodic overpotential is sufficiently large, the cathodic current is negligible. Thus, Eq. 1 can be simplified into Eq. 2, the logarithm form of which is the Tafel equation (Eq. 3).[4,23,24] For a multi-step electrochemical reaction, the Tafel slope (Eq. 4) may provide information of the reaction mechanism. Assuming that a rate-determining step (RDS) exists, the Tafel slope can be described as Eq. 5.[4,23,25]

$$j = j_0\left[\exp\left(\frac{\alpha_a nF\eta}{RT}\right) - \exp\left(-\frac{\alpha_c nF\eta}{RT}\right)\right] \tag{1}$$

$$j = j_0 \exp\left(\frac{\alpha_a nF\eta}{RT}\right) \tag{2}$$

$$\log j = \log j_0 + \frac{\eta}{b} \tag{3}$$

$$b = \frac{\partial \eta}{\partial \log j} = \frac{2.303RT}{\alpha nF} \tag{4}$$

$$\alpha_a = n_r\beta + \frac{n_b}{\upsilon} \tag{5}$$

where n_b is the number of electrons transferred before the RDS, υ is the number of rate-determining steps, n_r is the number of electrons that participate in the rate-determining step, and β is the transfer coefficient of the RDS (typically assumed to be 0.5). Eq.5 provides a simple yet rapid means to identify the RDS of OER. This simple treatment, however, is not sufficient to account for the real kinetic behaviors of OER catalysts. The same Tafel values may originate from different reaction pathways. Moreover, the treatment assumes a low coverage of the surface intermediate before the RDS, which does not always hold especially at high overpotentials. The transfer coefficient can deviate from 0.5 when the reorganization energy is comparable to overpotential, or when there is a significant barrier in the electron transfer.[26,27] Due to these limitations, a full kinetic analysis, including rate order determinations, in addition to Tafel analysis, is necessary to establish the detailed reaction mechanism.[22,23,26] Another important tool is first-principle DFT simulations of Tafel kinetics,[23] which gives fundamental information about the reaction mechanism.

3. Descriptor

The involvement of multiple intermediates makes the full kinetic description of OER on metal oxides a daunting task. There are significant efforts to correlate OER activity with a single macroscopic parameter, or descriptor.[11] The descriptor could be either an experimentally determined parameter, or a computed property. A good descriptor leads to a volcano-type relation of the activity of OER catalysts as a function of that descriptor. Identification of a good descriptor may give insights into the key step of the OER and be applied to accelerate the screening of new catalysts.

The first attempt to correlate the OER activity of metal oxides with a descriptor is traced back to 1955 in the work of Riutschi and Delahay.[28] They demonstrated an approximate linear correlation between the rate of oxygen evolution and the M-OH bond energy, suggesting M-OH bonding strength as a descriptor. By taking both the absorption and desorption of oxygenated intermediates into account, Trasatti demonstrated the enthalpy change for the lower-to-higher oxide transition ($MO_x \rightarrow MO_{x+1}$) as a descriptor. A 'volcano-shape' correlation of OER activity with this descriptor was obtained, with IrO_2 and RuO_2 at the top of the volcano.[29,30] One limitation of these studies is the sometimes inaccurate values of catalytic activity, M-OH bonding strength, and enthalpy change determined at that time.

Recently modern analytical techniques have been used to obtain more precise parameters. Markovic et al. studied near-monolayer (oxy)hydroxide films on single-crystal Pt support, and established $OH-M^{2+\delta}$ bond strength ($0 \leq \delta \leq 1.5$) as a descriptor.[31] They determined the $OH-M^{2+\delta}$ bond strength by measuring the CO oxidation rate on Pt, assuming a bifunctional mechanism where CO is exclusively absorbed on Pt while OH is absorbed only on metal oxides. The $OH-M^{2+\delta}$ bond strength followed the order of Ni<Co<Fe<Mn, which correlated well with the OER activity order (Ni>Co>Fe>Mn). Trace amounts of Fe impurities in commercial NaOH and KOH electrolytes

significantly increase the OER activity of NiO_x.[19,32] Boettcher revisited the activity trend of first-row transition metal oxyhydroxides after eliminating incidental Fe incorporation. They used thin film catalysts electrodeposited on Au and Pt electrodes through the nitrate reduction route. A modified activity order of $Ni(Fe)O_xH_y > Co(Fe)O_xH_y > FeO_xH_y\text{-}AuO_x > FeO_xH_y > CoO_xH_y > NiO_xH_y > MnO_xH_y$ was obtained.[33]. Our group recently developed an anodic deposition method for thin films of transition metal oxides (oxyhydroxides).[34] The intrinsic activity of these catalysts could be determined after filtering out deviations due to irregular surface area generations. The activity correlated with the M–OH bond strength proposed by Bockris and Otagawa,[34,35] and a volcano-type plot was obtained using this bond strength as a descriptor (**Figure 2a**). NiO_x and CoO_x were on the ascending branch, where the M-OH energies were lower than optimal. FeO_x and MnO_x were on the descending branch, where the M-OH energies were too strong. $NiFeO_x$ and $CoFeO_x$ sat at the top of the volcano thanks to near optimal M-OH bond strengths. The superior activity of $NiFeO_x$ and $CoFeO_x$ compared to unary oxides could be explained by considering a compromise of too weak and too strong M-OH bond strengths of their unary components. We then used this volcano-plot to design a new OER catalyst, $CoVO_x$, as Co and V also sat on two opposite branches of the plot.[36]
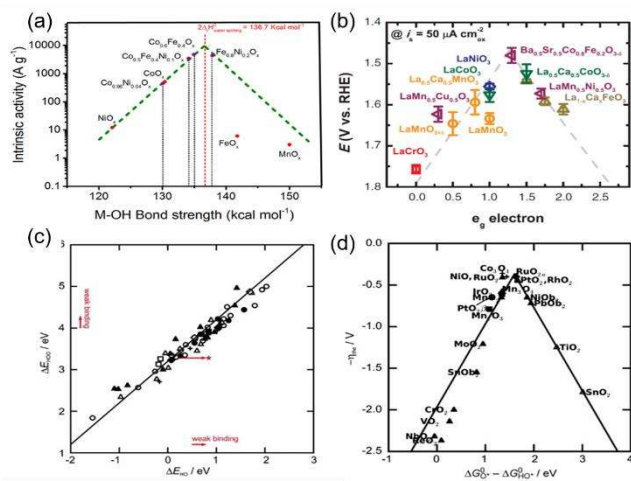

Figure 2. (a, b) Volcano plot of the intrinsic activities against descriptors of: (a) the M−OH bond strength in transition metal (oxy)hydroxides. Reprinted with permission from Ref. [34]. Copyright 2016 American Chemical Society. (b) The occupancy of the e_g-symmetry electron of the transition metal (B in ABO_3). Reprinted with permission from Ref. [39]. Copyright 2011 AAAS. (c) The universal scaling relation between adsorption energies of HO* and HOO* on perovskites, rutiles, anatase, Mn_xO_y, Co_3O_4, and NiO oxides. Reprinted with permission from Ref. [43]. Copyright 2011 Wiley-VCH. (d) Volcano plot of the calculated activities against descriptor of the $\Delta G_{O*}-\Delta G_{HO*}$ for rutile, anatase, Co_3O_4, Mn_xO_y oxides. Reprinted with permission from Ref. [43]. Copyright 2011 Wiley-VCH.

Electronic structure parameters have been applied as descriptors for perovskite catalysts. Bockris correlated the activity of perovskites with the number of 3d electrons of the transition metal ions in bulk perovskites.[35,37] A linear reactivity scale was obtained, which was rationalized by molecular orbital theory. Electrons from the d-orbitals occupy the antibonding orbitals of the M-OH bond. As the number of the d electrons increase, the bond strength of M-OH decrease, and the OER activity increase. A similar d-band model was used to rationalize the high

activity of a Co-C_3N_4 catalyst.[38] Shao-Horn proposed surface filling of e_g orbitals as an improved descriptor of the activity of perovskites (**Figure 2b**).[39] Compared to 3d electrons counts, e_g filling is in principle more appropriate because the e_g orbitals have more direct overlap with the oxygen-related adsorbate than t_{2g} orbitals. Moreover, as electrocatalysis occurs at the surface, a surface-based parameter is more accurate than a bulk parameter. A volcano plot was obtained using the e_g filling as a descriptor, with the optimal value being close to unity. $Ba_{0.5}Sr_{0.5}Co_{0.8}Fe_{0.2}O_{3-\delta}$ (BSCF) had a near optimal e_g filling, and it was indeed the best perovskite catalyst. For perovskites whose e_g filling is hard to estimate, e.g., double perovskites with multiple transition metal sites, Shao-Horn proposed the computed O p-band center relative to the Fermi level as an alternative descriptor.[40]

Although OER involves multiple steps and intermediates, descriptors related to absorption energy of a single intermediate, e.g, the M-OH bond strength, appear to work. The underlying reason is that the binding energies of the different intermediates (HO*, O* and HOO*) are linearly correlated. Rossmeisl et al. first showed computationally this correlation for metals, and then for rutile-type oxides (RuO_2, IrO_2, and TiO_2).[41,42] The same group recently revisited the trends of OER activity using an extensive database of calculated binding energies on surfaces of a large number of rutile, perovskite, spinel, rock salt, and bixbyite oxides.[43] A universal scaling relationship between HO* and HOO* was found for all the studied materials, as the difference between the adsorption energies of HO* and HOO* was always approximately 3.2 eV (**Figure 2c**). Based on this result, they proposed the energy of the reaction step ($\Delta G_{O*}-\Delta G_{HO*}$) as a universal descriptor for all oxides and perovskites. A volcano plot of the theoretical OER activity as the function of this descriptor is shown in **Figure 2d**. An interesting result originated from the universal scaling relationship is that there is a lower limit for the OER overpotential of metal oxides. The HO* and HOO* intermediates are separated by two proton and electron transfer steps; the perfect energy separation should be 2.46 eV. The constant difference of 3.2 eV suggests that the minimal overpotential is about 0.4 V, with an uncertainty of 0.2 eV. The minimal overpotential is achieved by catalysts with a ($\Delta G_{O*}-\Delta G_{HO*}$) of about 1.6 eV, which are located at the top of the volcano plot. To avoid the activity limitation imposed by the scaling relationship, the energy difference between HOO* and HO* need to be lower than 3.2 eV. In other words, HOO* need to be stabilized compared to HO*. Follow-up theoretical studies suggest that this might be achieved by the addition of a proton-acceptor functionality to RuO_2 and transition metal doped graphene, with the latter being a hypothetical catalyst.[44,45]

The descriptor approach greatly simplifies the understanding of the trends in the OER activity of metal oxides. Despite this progress, there are still unresolved critical issues: (1) The difficulty to accurately measure intrinsic catalytic activity and experimental descriptors. (2) The assumptions about the structures and active sites of catalysts can be erroneous. (3) It is difficult to correlate theoretical and experimental activity. (4) Theoretical descriptions of realistic conditions (solvent, electric field, etc.) and kinetics remain challenging. In a sense, the success of the descriptor approach depends on accurate knowledge of catalysts. Therefore, the descriptor approach will not replace, but rather require experimental approaches to define the structure, activity, and mechanism of catalysts.

4. Activity metrics

Activity metrics are required to quantitatively compare the activity of different OER catalysts. We recommend the following four activity metrics including turnover frequencies (TOFs), specific current density (J_s), geometric current density (J_g), and overpotential (η).

TOF is defined as the number of O_2 molecules a catalytic site evolves per unit of time, often second. In principle TOF is the best measure of the intrinsic catalytic activity. However, accurate determination of TOF is not straightforward because the true active sites of heterogeneous catalysts are very difficult to determine. A more realistic method to calculate TOF is to consider all relevant metal sites as active sites. The TOFs determined in this way surely represent only a lower limit of the true TOFs, nevertheless, they enable a fair and consistent comparison among catalysts prepared by different groups. Moreover, mass-averaged activity is highly relevant for industrial applications. Considering that TOFs are typically a function of potential, the overpotentials at which TOFs are measured must be reported. The TOFs for some typical metal oxides $\eta = 300$ mV are 0.03 s^{-1} for $Ni_{0.8}Fe_{0.2}O_xH_y$,[46] 0.02 s^{-1} for $Co_{0.54}Fe_{0.46}(OOH)$,[47] 0.002 s^{-1} for FeO_x,[48] 0.001 s^{-1} for CoO_x,[47] 0.0009 s^{-1} for NiO_x,[33] and 0.0004 s^{-1} for MnO_x.[49]

The specific current density (J_s) is an alternative metric for the intrinsic activity of electrocatalysts. J_s is defined as the current density at a specific overpotential normalized by the active surface area of the catalyst. This metric complements the TOF metric as inaccessible bulk sites are no longer counted. Accurately measuring the active surface areas is difficult.[50] The surface areas deduced from the capacitances of catalysts deposited on electrodes are often inaccurate because the specific capacitance can vary widely depending on surface chemistry, conductivity and porosity. Therefore, cautions need to be executed when compare specific current densities of different type of catalysts.

In part due to substantial work required for the measurement of TOF and J_s, researchers in the field tend to employ two other, more easily determined metrics to compare OER activity: geometric current density (J_g) at a specific overpotential and overpotential (η) for a specific geometry current density. These parameters are readily obtained from electrochemical data (e.g., CV or electrolysis). Recently in work aiming at solar energy storage, η (10 mA cm^{-2}) is widely used as the activity metric, because 10 mA cm^{-2} is the current density from a solar conversion device with 12% solar to hydrogen efficiency, which seems to be at the upper end of a conceivable goal. η for higher current densities (e.g., 500 mA cm^{-2}) is more relevant to electrolyzers.

Both η and J_g depend heavily on catalyst loading and electrode configuration (flat or porous). Generally, activity increases (lower η or higher J_g) when the loading increases until other factors such as conductivity, hindered mass transport, and aggregation of catalyst start to undermine the activity. At a same loading, a porous electrode tends to give higher J_g or lower η than a flat electrode due to better dispersion of catalyst, thus, higher surface area. For a meaningful comparison using η or J_g, we suggest that catalyst loading and the nature of electrode should be reported.

In the literature, Tafel slope is often used as an activity metric. The Tafel slope is an important electrokinetic parameter that reveals the dependence of the current density on the overpoten-

tial. A lower Tafel slope can be desirable because a faster increase in J_g can be obtained when applying a same amount of additional overpotential. However, Tafel slope is dictated by the catalytic mechanism for an ideal system, and influenced by conductivity of catalyst in actual systems, so the slope alone is not a recommendable activity metric. Comparison of η or J_g under a wide range of operating conditions already takes account of contributions from different Tafel slopes.

Even with commonly agreed activity metrics, fair comparisons of different OER catalysts are a difficult task using literature data, because catalytic activity is measured at a range of pH values, temperatures, electrolyte compositions and concentrations, and using different electrodes. Seemingly the same catalyst can have very different activity in two different reports. To address this issue, benchmarking efforts using internally consistent protocol was conducted on a range of metal oxide OER catalysts.[51-53] In these studies, η, J_g, and J_s were used as the activity metrics. Considering the dynamic nature of OER catalysts under operating conditions, Boettcher et al. reported a series of procedures and measurement techniques that could assess the potential-induced phase transitions, potential-dependent electronic properties, variable oxidation and protonation states, and disordered local/surface phases of oxide catalysts.[46] According to these benchmarking studies, $NiFeO_x$ stands out as a non-precious, highly active, and stable OER catalyst in alkaline solutions.

Statistical analysis has so far been overlooked when the activity of OER catalysts is reported. Without a proper statistical analysis, it is difficult to evaluate the uncertainty and reproducibility of activity measurements. Consequently, comparison of different catalysts becomes problematic. There might be no statistical difference between a TOF of 0.02 s^{-1} and a TOF of 0.03 s^{-1}, if the standard deviation is sufficiently large. We recommend reporting sample size and standard errors as a good practice in electrocatalytic studies.

5. In situ and operando characterization

In situ and operando characterization of surface electrocatalysts are technically challenging due to the heterogeneous nature of the catalysts, the liquid-phase reaction medium, the bubble-evolving gaseous product, and the electrochemical interface.[54] Several reviews have already summarized recent in situ and operando studies of metal oxide-based OER catalysts.[4,54-56] Only a few representative studies are recapitulated here (**Figure 3**).

X-ray absorption spectroscopy (XAS) is a powerful tool to probe the chemical, electronic and structural information of electrocatalysts (**Figure 3a**).[57] In situ and operando XAS has been employed to track changes in oxidation state, coordination geometry, and bond length of $NiFeO_x$.[58-60] Friebel et al. obtained in situ XAS data to establish the local environment of Ni and Fe cations in $Ni_{1-x}Fe_xOOH$.[58] The oxidation states of Ni and Fe in the as-prepared samples were as +2 and +3, respectively, independent of the amount of Fe. As the potential was increased beyond the OER onset, the Ni cations were oxidized to Ni^{3+} while the Fe cations remained as Fe^{3+}. They concluded that samples with less than 25% Fe, which were more active, were Fe-doped NiOOH, in which Fe^{3+} occupied octahedral sites with unusually short Fe-O bond distances. Görlin et al. investigated metal redox states and local structure motifs mixed Ni-Fe oxides using quasi-in situ XAS (quasi-in situ means the catalyst films were first subjected to OER potentials, freeze-quenched in liquid N_2, and then analyzed ex-situ as dry samples).[59] They observed that

up to 75% of the Ni centers changed from Ni^{2+} to Ni^{3+}, while up to 25% arrived at Ni^{4+} for NiOOH under OER conditions. For $NiFeO_x$, the Fe centers remained as Fe^{3+}, regardless of the potential and composition. However, the Ni ions largely remained as Ni^{2+} under catalytic conditions. The low level of oxidized Ni in $NiFeO_x$ was reconciled by considering a kinetic competition between the metal oxidation process before oxygen evolution and the metal reduction step during O_2 release. Nocera et al. used in situ Ni K-edge XAS and O K-edge electron energy loss spectroscopy (EELS) to study the oxidation state of Fe-doped Ni oxide.[68] Previously they observed Ni^{4+} in NiOOH type catalysts. They observed a decreased in Ni K-edge energy of about 0.8 V in Fe-doped Ni oxide, less than Görlin et al. (about 2 eV) in $NiFeO_x$. This energy decrease was not assigned to reduction of Ni as proposed by Görlin et al., but to an increased Ni-O covalency. According to electronic structure considerations, the increased Ni-O covalency was correlated to higher formal Ni(IV) character. Thus, the authors proposed that Fe doping promoted the access to Ni(IV). These three XAS studies of seemingly similar catalysts give rather different information about the oxidation states of Ni and Fe, which in turn leads to different hypotheses of their active site (see **Section 6**). This discrepancy indicates the challenge in the interpretation of XAS data, in addition to filtering deviations caused by different sample compositions and measurement conditions.
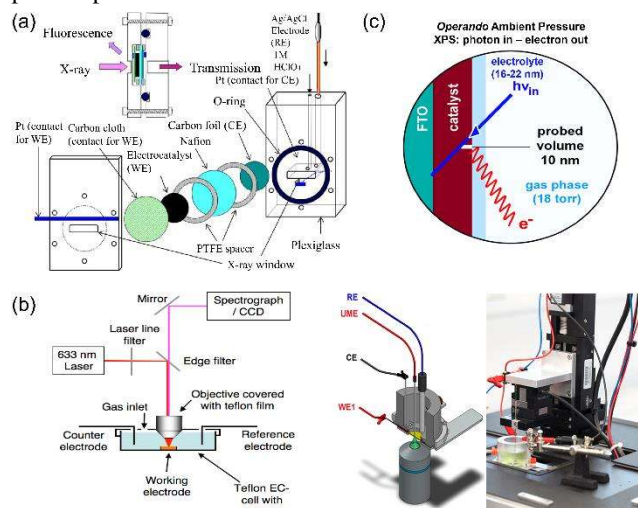

Figure 3. (a) A scheme of electrochemical cell used for in-situ XAS analysis. Reproduced with permission from Ref. [57]. Copyright (2010) Elsevier. (b) (Left) A schematic diagram of the in situ SERS electrochemical set-up and (Right) a scheme and picture of the installed SECM instrument used for the in situ measurements. Reproduced with permission from Ref. [65] Copyright (2011) American Chemical Society and Reproduced with permission from Ref. [66]. Copyright (2017) American Chemical Society. (c) A schematic representation of AP-XPS used for the operando investigation of OER electrocatalysts. Reproduced with permission from Ref. [69]. Copyright (2016) American Chemical Society.

In an interesting example, the function of different geometrical sites in spinel cobalt oxide was distinguished by in situ XAS.[61] The experiments were done on modified Co_3O_4 samples where the tetrahedral site (Co^{2+}_{Td}) and octahedral site (Co^{3+}_{Oh}) were substituted by inactive Zn^{2+} and Al^{3+}, respectively. The study suggested that $Co^{2+}_{(Td)}$ was the active site for OER while $Co^{3+}_{(Oh)}$ only contributed to surface double layer capacitance.

Mössbauer spectroscopy has been applied to analyze Fe-containing catalysts.[62,63] Stahl et al. observed Fe^{4+} species in $NiFeO_x$ by operando Mössbauer spectroscopy.[63] These Fe^{4+} sites were kinetically incompetent as active sites in OER, but their presence pointed to the possibility of more active, unobserved Fe^{4+} species located at the edge, corner, or related defect sites as the active sites. The inability to capture such active Fe^{4+} species reveals an important limitation of Mössbauer spectroscopy, which is its low sensitivity even for ^{57}Fe enriched samples.

Both XAS and Mössbauer spectroscopies employ high energy irradiations which can readily penetrate through the liquid medium and into the bulk materials. As catalysis occurs at the surface, more surface-sensitive spectroscopy is desirable.

Modern Raman spectroscopy covers the whole spectral range from 100 to 4000 cm^{-1} and is easily adapted for in situ measurements.[64] Thus, Raman spectroscopy is widely used in the in situ and operando studies of OER catalysts (**Figure 3b**).[65-68] Bell et al. used in situ surface-enhanced Raman spectroscopy (SERS) to investigate CoO_x deposited on Au and other substrates (**Figure 3b**).[65] They found that the as-prepared CoO_x was Co_3O_4, which was transformed to CoOOH upon applied potential. Au was the best substrate compared to Pt, Pd, Cu and Co. The enhanced activity of Au was attributed to an increased population of Co(IV), which was proposed to beneficial for OER. Using SERS, Smith et al. obtained evidence for a so-called adsorbed active oxygen species ($NiOO^-$) on $NiFeO_x$.[68] This species has a broad Raman peak in the region 900-1150 cm^{-1}. Although the chemical identity of this species is still unclear, they proposed that it was formed by a deprotonation process that depended on the pH of the electrolyte. The formation of this species seems to support Ni as the active site in $NiFeO_x$ (see **Section 6**).

Conventional X-ray photoelectron spectroscopy (XPS) requires ultra-high vacuum (UHV) conditions. Recent developments of ambient pressure X-ray photoelectron spectroscopy (AP-XPS), coupled with synchrotron radiation sources, have enabled in situ XPS studies of OER catalysts (**Figure 3c**).[69] Friebel et al. characterized $NiFeO_x$ using operando AP-XPS.[70] Due to ohmic losses in the electrode/electrolyte system, their method only allowed the operando studies at low current densities, where the potentials were just above the onset for OER. Under these conditions, they showed that a thin film of $NiFeO_x$ electrochemically deposited on Au initially comprised of metallic Ni and Fe as well as their oxides. The metal ions were further oxidized upon electrochemical cycling, reaching $Ni^{2+/3+}$ and Fe^{3+}. The authors proposed alternative approaches to investigate the catalysts under realistic current densities (e.g., 10 mA cm^{-2}). Favaro et al. combined in situ XAS and AP-XPS to study a quinary oxide catalyst $(Ni-Fe-Co-Ce)O_x$.[69] The AP-XPS data suggested that at low current densities the electrochemical performance of Ni, Co, and Fe were oxidized from +2 in the as-prepared sample to active (Ni,Fe,Co)(III)O(OH) species, although the oxidation of Ni and Co is partial. They also found that the changes in the surface of the catalyst was quite different from the changes in the bulk. While CeO_2 was redox inactive, it influenced the redox processes of the transition metals and boosted the catalytic activity at low overpotentials.

In situ and operando microscopy has also been developed for the studies of OER catalysts.[66,71,72] Boettcher et al. employed operando electrochemical atomic force microscopy (EC-AFM) to investigate the dynamic changes of single-layered $Ni(OH)_2$

nanosheets during catalysis (see also **Section 7.1**).[71] Morphology, surface area, and volume changes were observed. Moreover, heterogeneous Fe incorporation was revealed, which was an important finding for the understanding of NiFeO$_x$. Bard et al. used surface interrogation scanning electrochemical microscopy (SI-SECM) to probe the kinetics of surface Ni and Fe sites in NiOOH, FeOOH, and NiFeO$_x$ (see also **Section 6**).[72] Bron et al. combined Raman microscopy with SI-SECM to provide both spectroscopic and electrochemical information on the very same location of an electrocatalyst (**Figure 3b**).[66] They demonstrated the utility of this method for the study of NiOOH and NiFeO$_x$. The incorporation of Fe introduced structural disorder which was essential for the high OER activity of NiFeO$_x$.

It is now well established that the composition, morphology, oxidation state of metal ions, and intermediates of metal oxides depend critically on the applied potential and reaction conditions. Therefore, in situ and operando characterization is indispensable for the understanding of these catalysts and their reaction mechanism. Because access to synchrotron facility is restricted for most researchers, benchtop in situ and operando tools are highly desirable. Improvement of temporal and point resolution is another important objective.

6. Active site of Fe-containing mixed metal oxides

FeO$_x$ alone has low OER activity, but even a trace amount of Fe ion significantly increase the activity of Ni or Co (oxy)hydroxides.[19,32,47] Fe increases the activity of Co and Ni (oxy)hydroxides by up to 30- and 1000-fold, respectively. It is now widely accepted that the high activity sometimes observed with NiO$_x$ is due to incidental incorporation of Fe ions present as impurities in the commercial electrolyte medium (**Figure 4a**).[32,73] There is not yet consensus whether Fe incorporation is always responsible for highly active CoO$_x$ catalysts.[34,47] In any case, NiFeO$_x$ and CoFeO$_x$ are among the most active OER catalysts in alkaline solutions, much more active than the corresponding unary oxides.[32,34,47] The element nature of the active site in NiFeO$_x$ and CoFeO$_x$ is actively debated in the field.

The promoting effect of Fe on Ni(OH)$_2$/NiOOH was discovered by Corrigan in the 1980s.[19] It was hypothesized that increased conductivity due to Fe incorporation and the electron-withdrawing effect of Fe on Ni were responsible for the promotion.[19,62] Boettcher revisited Fe doped Ni/Co oxyhydroxides, and found neither the conductivity nor electron-withdrawing effect was sufficient to explain the dramatic enhancement of activity upon Fe incorporation.[32,47,74,75] By eliminating Fe impurities from electrolytes, they were able to obtain "clean" TOFs of FeOOH, CoOOH, and NiOOH. FeOOH is actually more active (TOF = 0.016 ± 0.003 s^{-1} at η = 350 mV) than CoOOH (TOF = 0.007 ± 0.001 s^{-1} at η = 350 mV) and NiOOH (TOF ≈ 0.01 s^{-1} at η = 400 mV). Moreover, FeOOH is an insulator under OER conditions, while NiOOH ($\sigma \approx$ 0.1 to 0.2 mS cm^{-1}) and CoOOH ($\sigma \approx$ 4 mS cm^{-1}) are conductive.[32,47] Based on these results, they proposed that Fe is the active site in NiFeO$_x$ and CoFeO$_x$, and NiOOH or CoOOH mainly serves as an electrically conductive and chemically stable host for the Fe sites. Boettcher then studied the effects of La, Mn, Ce, and Ti incorporation on the activity and redox behavior of Ni (oxy)hydroxide, NiO$_x$H$_y$.[74] Only Ce increased the activity of NiO$_x$H$_y$ (by about 10-fold), but the effect was transient. No correlation between activity and the nominal Ni^{2+}/$^{3+}$ redox potential was found. These results underscore the uniqueness of Fe, and is consistent with it being the active site in NiFeO$_x$. The same group then reported evidence

for different types of Fe species in NiFeO$_x$: those rapidly incorporated upon contact with an iron source and those required more time for incorporation.[75] The former likely locate at edges or defects of the material while the latter likely substitute Ni in the bulk material. Only the former type of Fe species is responsible for the enhanced OER activity, whereas the latter type modulates the observed Ni voltammetry but not the activity.
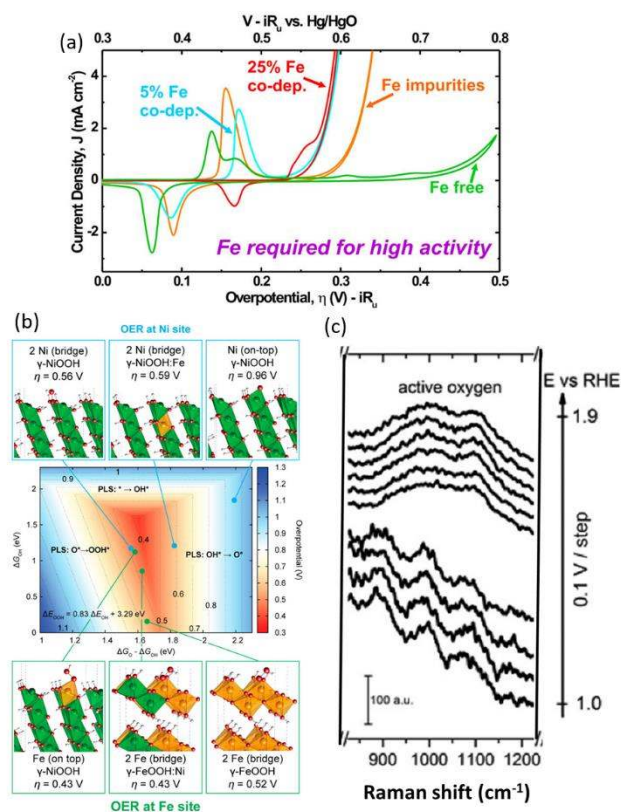

Figure 4. (a) CV scans of Fe contaminated Ni(OH)$_2$ and Ni$_{1-x}$Fe$_x$OOH films of different Fe contents deposited on IDA electrodes. Reprinted with permission from Ref. [32]. Copyright 2014 American Chemical Society. (b) Theoretical OER activity volcano showing the overpotential as a function of Gibbs free energies of the reaction intermediates at Ni and Fe surface sites in pure and doped γ-NiOOH and γ-FeOOH model structures. Reprinted with permission from Ref. [58]. Copyright 2015 American Chemical Society. (c) Surface-enhanced Raman spectroscopic evidence for the generation of adsorbed "active oxygen" (negatively charged NiOO$^-$ sites) in Ni(Fe)(OH)$_2$ acquired in the potential range 1.0−1.9 V vs RHE in 0.1 M KOH. Reprinted with permission from Ref. [68]. Copyright 2015 American Chemical Society.

One of the earliest evidences for Fe as the active site in NiFeO$_x$ was provided by DFT computations.[58] Using geometries established by an operando XAS study, computations revealed that the Fe site had a theoretical overpotential of about 0.43 V while the Ni site had an overpotential of 0.56 V (**Figure 4b**). Note that the overpotential for this Fe site approaches the minimal value predicted by previous DFT computations (see **Section 3**; Ref. 43) due to the universal scaling relationship. Ahn and Bard employed SI-SECM to direct measure the surface OER kinetics of Ni(IV) and Fe(IV) in NiOOH, FeOOH, and NiFeO$_x$ (see also **Section 5**). They found two types of surface sites with fast and slow kinetics, respectively.[72] The fraction of the fast site in NiFeO$_x$ matched its iron content. Thus, they concluded that the Fe(IV) site was the active site for OER, with a

TOF of 1.7 s^{-1} at η = 438 mV (0.6 V vs Ag/AgCl (1M Cl$^-$) in 2 M NaOH). As a comparison, the Ni(IV) site in NiOOH has a TOF of 0.04 s^{-1}, while the Fe(IV) site in FeOOH has a TOF of 0.18 s^{-1}. These results provided experimental support for the conclusion of the DFT study.[58] It is noted that redox titration employed in this study appears to catch the Fe(IV) oxidation state while XAS studies only detected Fe(III) even under OER conditions.[58,59,76] On the other hand, Fe(IV) was observed by an operando Mössbauer spectroscopic study (see also **Section 5**).[63] Interestingly, the observed Fe(IV) species (up to 21% of the total Fe) were not responsible for OER, and the authors proposed unobserved Fe(IV) species, likely at edge, corner, or defect sites, as possible active site. This proposal was echoed in the Boettcher study which revealed different types of Fe species in NiFeO$_x$ (see above).[75] A following combined DFT computational and spectroelectrochemical study further supported the role of Fe(IV) species in OER catalyzed by NiFeO$_x$.[77] Adding to the evidences that Fe is the active metal in NiFeO$_x$, the group of Gray and Winkler reported in situ spectroscopic measurements of NiFe layered double hydroxide (LDH) in nonaqueous medium and identified cis-dioxo-iron(VI) as the reactive intermediate.[78]

While an increasing number of studies favor the Fe active site mechanism, the Ni active site mechanism has some support as well. Negatively charged sites of NiOO$^-$ (described as adsorbed "active oxygen") was identified by in situ Raman spectroscopy studies of both NiOOH.[79] and NiFeO$_x$ catalysts[68] (**Figure 4c; see also Section 5**). The generation of these sites was linked to the OER activity. These studies did not rule out the Fe as the active site, but indicated that the formation of highly oxidized Ni sites played an important role in catalysis. In a quasi-in situ XAS study, Görlin et al. observed that Ni ion remained as Ni(II) in NiFeO$_x$, rather than being oxidized to Ni(III) and Ni(IV) in pure NiOOH (see also **Section 5**).[59] They hypothesized that high-valent Ni ions were reduced upon releasing O$_2$, thus, proposing Ni as the active site. The group of Nocera found that doping of Fe promoted the ability of Ni ion to access a Ni(IV) state at modest overpotentials (see also **Section 5**) They observed greater co-valency of Ni-O when the oxidation state of Ni is increased. Considering that Fe(III) is a very Lewis-acidic metal ion, they proposed the role of Fe is to promote the formation of Ni(IV) through a Lewis-acid effect.[60]

The difficulty in settling the element nature of the active site in NiFeO$_x$ and related CoFeO$_x$ might be attributed to the lack of direct, unambiguous detection of the active site. The presence of Fe(IV) or Ni(IV), and even its correlation with the activity, neither prove that such a site is an active site, nor exclude the alternative site assignment. Direct comparisons of site activity are made in several DFT computations which favor the Fe site mechanism.[58,77] Nevertheless, the computations are limited by assumptions of site structure as well as methodology. The SI-SECM study directly measured and compared the site activity of Ni and Fe sites, however, the assignment of the fast reaction site to Fe site was mainly based on the fraction of the fast site which was similar to the Fe content.[72] An alternative explanation is that only a Ni site activated by a neighboring Fe site becomes a fast site. Element specific characterization techniques together with improved, experimentally calibrated DFT computations are necessary to resolve this issue. Meanwhile, we propose an approximate, unifying treatment of the active site: an oxygen-bridged Ni-Fe dimer. This treatment takes into consideration that both Ni and Fe are essential for the activity, as well as the correlation of activity with active Fe content. According

to this treatment, the TOFs of NiFeO$_x$ (extendable to CoFeO$_x$) should be calculated based on Fe content (often less than Ni) which is the upper limit of the number of such dimeric unit.

7. Materials development

7.1 2D materials

Two dimensional (2D) materials have close to maximum surface to bulk ratio, and the surfaces are highly exposed. They generally have higher conductivity than their bulk counterparts as well. These features make 2D materials attractive for electrocatalysis.[80] 2D materials are also excellent building blocks for hierarchical, hybrid catalysts. Finally, 2D materials are more "molecularly" defined than 3D nanoparticles, as a result, structure-activity studies are simplified.
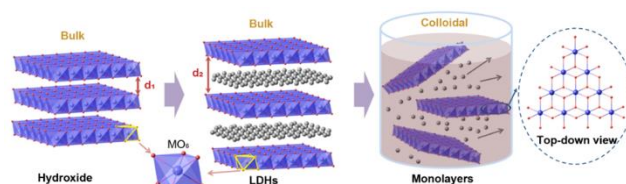

Figure 5. Schematic illustration of the exfoliation of bulk LDH to 2D catalysts. Reprinted with permission from Ref. [81]. Copyright, the authors.

2D OER catalysts can be synthesized following a 'top-down' strategy, that is, to delaminate layered 3D catalysts into mono- or few-layered species. Our group applied a liquid-phase exfoliation method to delaminate three bulk LDHs (NiFe, NiCo, and CoCo) into single-layered hydroxides (0.8 nm) (**Figure 5**).[81] The exfoliated LDH nanosheets exhibited 2.6-, 3.4- and 4.5-fold higher OER activity than their bulk counterparts in alkaline conditions. Both NiFe and NiCo LDH nanosheets were more active and stable than a commercial IrO$_x$ catalyst. We showed that surface area increase was not the main contributor to the enhanced activity; instead, a higher number of active sites, probably at the edges, were created through exfoliation. A similar exfoliation strategy was applied for Ni$_x$Co$_{1-x}$(OH)$_2$.[82-84] It was shown that breaking monolayer NiFe LDH into ultrafine nanosheets (2.3 nm in size) further improved its OER activity[85]. Water and Ar plasma techniques were employed to facilitate the exfoliation, and more importantly, to create multiple vacancies (Co, Fe, and O), of CoFe LDH.[86,87]

2D OER catalysts can also be directly synthesized from molecular precursors, i.e., via a 'Bottom-up' strategy. Our group developed a one-pot co-precipitation method to synthesize ultrathin nanoplates of CoMn LDH.[88] These nanoplates have an average thickness of 3.6 nm. Sun et al. developed a hydrothermal method for the synthesis of highly active NiV LDH monolayers.[89] 2D metal oxide and hydroxide catalysts were also obtained by annealing[90] or chemical oxidation[91] of ultrathin metal hydroxides, which were in turn prepared from molecular precursors.

The enhanced OER activity of 2D catalysts (compared to their 3D counterparts) was generally attributed to more abundant active sites and higher conductivity.[81] Xie correlated the OER activity with oxygen vacancies in spinel NiCo$_2$O$_4$ nanosheets.[92] Their DFT computations indicated that oxygen vacancies reduced the H$_2$O adsorption energy at Co^{3+}, which would lead to higher activity in their analysis. Plasma treatments were then successfully applied to create various vacancies in 2D catalysts.[86,87] Improved conductivity and structural

distortion of surface CoO_{6-x} octahedrons were proposed to lead to much higher activity of γ-CoOOH nanosheets compared to bulk CoOOH.[91] Improved conductivity was also proposed as a main contributor to the high activity of NiO and MnO_2 nanosheets.[93,94] Selective etching of Ga and Al ions from Ga- and Al-containing LDH nanosheets created porous structures and highly active OER catalysts.[95,96] The enhanced activity was proposed to result from a higher abundance of edge sites in the porous nanosheets.

The development of 2D OER catalysts is still limited by their synthesis. Direct synthesis of 2D oxides is difficult due to the screw dislocation-driven growth mechanism.[97] Exfoliation of layered oxides is currently the most commonly used method, however, exfoliation can create defects which can be difficult to detect and analyze. Given that defects are possible reaction sites, uncontrolled creation of defects, either in exfoliation or in post modification, makes meaningful structure-activity correlation difficult. Oxide catalysts undergo dynamic changes in composition, structure, and oxidation states of metals during OER. However, the majority of spectroscopic characterization of 2D catalysts is ex situ, pre-catalytic. In this sense, convincing experimental evidence for the role of conductivity and vacancy in catalysis has not been obtained for 2D catalysts. For practical applications, 2D catalysts need to be prepared easily, cheaply, and in large quantity, be integrated into relevant devices, and exhibit good system performance and stability. All these challenges make the studies of 2D OER catalysts an exciting research area.

7.2 High surface area catalysts

Porous metal oxides have high surface areas which can be beneficial for the OER activity. A template approach has been developed to prepare porous OER catalysts. For example, Yang et al. prepared mesoporous Co_3O_4 using porous silica as a hard template via a nanocasting route.[98] The mesostructured Co_3O_4 exhibited dramatically increased OER activity compared to bulk Co3O4 due to increased surface area increased. Cao et al. synthesized porous Ni-Fe mixed oxides by low-temperature (200 °C) removal of organic surfactant Tween 85.[99] The porous structure resulted in higher OER activity compared to samples prepared in the absence of Tween 85. Our group recently reported that Sn ions in perovskite hydroxide $CoSn(OH)_6$ nanocubes can be electrochemically etched away to form a hierarchical nanoporous CoO_x catalyst.[100] A current density of 10 mA cm^{-1} was obtained at an overpotential of only 274 mV. It was shown that oxygen vacancies promoted the selective etching of Sn.

High surface area metal oxides were also prepared using metal organic frameworks (MOF) as precursors in controlled heat treatments. Qiao et al. prepared Co_3O_4-C hybrid porous nanowire arrays by carbonization of Co-based MOF grown on Cu foil.[101] This material had a high surface area of 251 m^2 g^{-1} and a carbon content of 52.1 wt%. It could be directly used as an electrode and exhibited higher OER activity and stability than IrO_2/C.[101]

Directly growing metal oxides on porous metal substrates, such as nickel (Ni) foam, is another strategy to prepare high surface area OER catalysts. The metal substrate can serve as a highly conductive scaffold to overcome the poor electrical conductivity of metal oxides. Various synthetic methods such as hydrothermal/solvothermal reactions,[102-104] electrodeposition,[105,106] and chemical bath deposition,[63] have been employed to grow metal oxides on porous metal supports. Qiao et al. grew

N-doped NiFe LDH nanolayers on a 3D Ni foam. The resulting electrode had superior performance in OER, delivering 10 mA cm^{-1} at a low overpotential of 230 mV and exhibiting durability in more than 60 hours of operation.[63] The study indicated that the 3D conductive framework, ultrathin N–NiFe LDH nanolayer ($\approx$0.8 nm), and high N-doping content ($\approx$17.8%) all contributed to the catalytic performance. Li et al. prepared FeOOH/Co/FeOOH hybrid nanotube arrays supported on Ni foam for OER in alkaline media.[105] They proposed that the Co core served as an efficient conductive layer to overcome the poor conductivity of FeOOH. Their DFT computations indicated strong interaction between Co and FeOOH. The catalyst exhibited a high surface area. A current density of 20 mA cm^{-2} was obtained at η = 250 mV. The same group further synthesized MOF-74-Co/Fe nanorod arrays on Ni foam.[104] After calcination in N_2, 3D porous $CoFe_2O_4$/C nanorod arrays supported on Ni foam were obtained. This catalyst delivered 10 mA cm^{-2} at η = 240 mV.

7.3 Hybrid materials

Hybridizing metal oxides with carbon supports is an efficient strategy to enhance their OER activity. High specific surface area carbon supports enable the well dispersion and full use of supported catalysts, and facilitate electron-transfer kinetics. Dai et al. synthesized ultrathin NiFe LDH on mildly oxidized multiwalled carbon nanotubes through consecutive solvothermal treatments.[107] The hybrid catalyst had an overpotential of 0.29 V for 5 mA cm^{-2}, and was more active than NiFe-LDH alone and NiFe-LDH mixed with CNTs. It was proposed that direct growth of NiFe LDH led to strong interaction between NiFe LDH and CNT, which enhanced electron transport and facilitated OER. The groups of Strasser and Dau investigated the effects of conductive supports on the redox behavior and OER activity of Ni-Fe(OOH).[76] They found that the catalyst immobilized on Vulcan XC-72r had 2–3 fold higher activity compared to unsupported Ni-Fe(OOH) catalyst. The supported catalyst also had a lower Tafel slop. Spectroscopic analyses indicated that the carbon support induced a cathodic shift and enhancement of the catalyst redox wave in the precatalytic potential range. The support also enhanced OER activity by particle dispersion, allowing a larger population of active sites to become accessible.

Modification of carbon supports by heteroatom doping or functional group attachments has been applied to further enhance the catalyst-support interaction in OER catalysis. It was proposed that the heteroatom or group might create favorable binding site to metal oxides, or even bind to catalytic intermediates. Qiao et al. prepared a 3D hydrated catalyst by growing NiCo double hydroxides on N-doped graphene (NG) hydrogels.[108] The NG-NiCo exhibited higher activity than NiCo double hydroxides grown on graphene and IrO_2. The authors proposed that synergy of N-doped graphene and NiCo hydroxide contributed to the high activity, but due to many other factors this effect was not directly confirmed. By anchoring crystalline β-Ni(OH)$_2$ onto oxidized CNTs,[109] Sun et al. found that oxygen functional groups on CNT surface significantly promoted OER catalysis of Ni(OH)$_2$. The hybrid catalyst had an overpotential of 270 mV at 10 mA cm^{-2}. The authors proposed that these oxygen groups facilitated proton-coupled electron transfer.

8. Stability studies

High catalytic activity is not sufficient for an OER catalyst to be applied in a real-life water splitting device. The catalyst

needs to exhibit long-term stability. In the literature, the stability of a metal oxide catalyst is commonly studied by potentiodynamic, chronoamperometric, or chronopotentiometric experiments during a few hours. The activity profile of the catalyst is then used as an indication of its stability. For example, in a benchmarking study, McCrory et al.[51] used a protocol based on electrolysis at 10 mA cm^{-2} during 2 hours to assess the short-term stability of OER catalysts in alkaline solutions. While many oxides were stable under these conditions, $CoFeO_x$ was less so, and IrO_x was very unstable. The overpotential of an IrO_x thin film increased from 0.32 to 1.05 V. The authors noted the limitation of this short-interval protocol and the need for other long-term testing methods. An example of long-term stability test under forcing conditions was provided by Sivula et al., who showed that Gibeon meteorite had a stable performance at 500 mA cm^{-2} for up to 1000 h.[110] It should be noted that Ni-based catalysts usually have an activation process during activity-based stability tests, due to incidental incorporation of Fe impurities (see **Section 6**).

Stable OER activity does not necessary indicate a stable catalyst because a catalyst can lose part of its mass while maintaining the same level of activity. The mass change of the catalysts during OER is an important information related to its stability. To monitor in situ the possible mass change during OER, electrochemical quartz crystal microbalance (eQCM) has been used.[111] Based on the inverse piezoelectric effect and with a high sensitivity factor, eQCM has a detection limit of 1 ng.[111] Boettcher et al.[33,48] employed eQCM to monitor the mass changes of metal oxides during short-term electrolysis (e.g., 4 h) in alkaline solutions at modest overpotentials (e.g., 350 mV). They found that under the conditions where the current densities were at 1-10 mA cm^{-2}, Ni- and Co-containing oxides (with or without Fe) appeared to be stable but FeOOH was unstable. They also found that the stability of $Co_{1-x}Fe_xOOH$ depended on the amount of Fe. For $0 < x < 0.5$, the catalyst was stable according to eQCM; for $0.5 < x < 1$, however, 18−38% of mass loss was detected.[47] They suggested that for $Co_{1-x}Fe_xOOH$ with a high Fe content, isolated and unstable FeOOH domains existed.

The mass change in eQCM is sometimes caused by factors other than dissolution or re-deposition of catalysts, e.g, by intercalation of ions.[112] Elemental analysis by inductively coupled plasma (ICP) spectrometry is more reliable for detecting the mass change of the catalysts, but it is normally not adaptable for continuous, in situ monitoring. Frydendal et al. combined eQCM and ICP-MS to study the stability of RuO_x and MnO_x.[113] They performed chronopotentiometric and chronoamperometric electrolysis for 2 h. The dissolution rate of RuO_x was about 4 monolayers per hour in acid, and that of MnO_x was similar in alkaline solutions. The authors noted that eQCM and ICP-MS gave different results, but the trends were similar. The results from ICP-MS were deemed more reliable. Mayrhofer et al. developed a setup comprised of an electrochemical scanning flow cell (SFC) connected to an ICP-MS to study the stability of OER catalysts.[114] They found that independent of the electrolytes (acidic or alkaline), OER activity decreased as Ru > Ir ≈ RuO_2> IrO_2, while dissolution increased as IrO_2 << RuO_2 << Ir << Ru.[114] The stability of RuO_2 and IrO_2 were 2–3 orders of magnitude higher compared to their metal counterparts, and the stability of all four compounds was higher in acidic than in alkaline solutions.

Spanos et al.[115] used a similar setup comprised of an electrochemical flow cell coupled with ICP- optical emission spectrometry (OES) to monitor the corrosion profiles of $NiCoO_2$, ordered mesoporous Co_3O_4 and $Fe-Co_3O_4$ during a stability testing protocol. Little, if any, metal corrosion was found in a 2 h test.

As pointed out in a recent paper,[116] the currently often used activity-based stability tests during a short time interval have many limitations including inability to detect catalyst degradation and its mechanism. In situ methods probing the changes in mass, surface area and conductivity are necessary in order to establish a comprehensive stability profile. This goal might be achieved by the combination of several independent methods such as eQCM, ICP, flow cell, and impedance spectroscopy.

9. Selected photoelectrochemical applications

Much of the research in OER catalysis is motivated by the possibility to store solar energy using water splitting. Besides photovoltaic-driven water electrolysis, photoelectrochemical (PEC) water splitting is proposed as an alternative approach to solar hydrogen production. Metal oxides and hydroxides have been applied as catalyst layers to enhance the PEC performance of photoanodes. Selected examples operating in alkaline solutions are discussed here.

Hu *et al.* stabilized Si, GaAs and GaP photoanodes using conformal and hole-conductive TiO_2 coatings for operation in 1M KOH. Using NiO_x islands as an OER catalyst, these systems showed maximum photocurrents of >30, 14.3 and 3.4 mA·cm^{-2} for Si, GaAs and GaP photoanodes, respectively.[117]

N-type $BiVO_4$ is an intensively studied oxide photoabsorber, which has a suitable valence band positioning for OER. This material is not stable in alkaline media and has mostly been investigated in neutral or near-neutral conditions.[118] Lichterman *et al.* reported a $BiVO_4$ photoanode coated by a layer of CoO_x. The CoO_x layer acted as both a protective and a catalyst, so the system operates at pH = 13 (**Figure 6a**).[119]

Hematite (α-Fe_2O_3) is another oxide semiconductor that drew attention due to its favorable bandgap, band positioning, abundancy, non-toxicity and stability in alkaline condition (pH 14). Metal oxide catalysts are frequently used to enhance the PEC performance of hematite. The most commonly used catalysts are CoO_x, NiO_x, and $NiFeO_x$. The catalyst integration has been achieved using electrodeposition, photoelectrodeposition, atomic layer deposition (ALD), hydrothermal growth, drop casting, and dip-coating.[120] ALD of CoO_x led to a submonolayer catalyst on an inverse opal hematite photoanode.[121] A significant cathodic shift of 100-200 mV in photocurrent was obtained (**Figure 6b**). It was shown that the addition of only 1 ALD cycle reduced the charge transfer resistance, leading to faster OER kinetics. Wang deposit $NiFeO_x$ on hematite using a photodecomposition method previously developed by Berlinguette.[122,123]Significant cathodic shift of the photocurrent was achieved, however, the catalyst layer was thick and absorbed strongly the light. As a result, backside illumination was necessary.

Parasitic light absorption by the OER catalysts has been recognized as a challenge in solar water splitting.[124,125] Our group developed an optically transparent $FeNiO_x$ catalyst.[126] This catalyst was deposited on flat and nanostructured hematite photoanodes. No obvious change in transmittance was observed upon coating of the $FeNiO_x$ catalyst. A cathodic shift of 200 mV

of the onset potential of OER was achieved by using this catalyst (**Figure 6c**). The optical transparency of the catalyst allowed the construction of a stacked tandem cell device comprised of a hematite photoanode and an underlying perovskite solar cell. Unassisted solar water splitting was achieved using this device, with a solar-to-hydrogen efficiency of about 1.9 %.
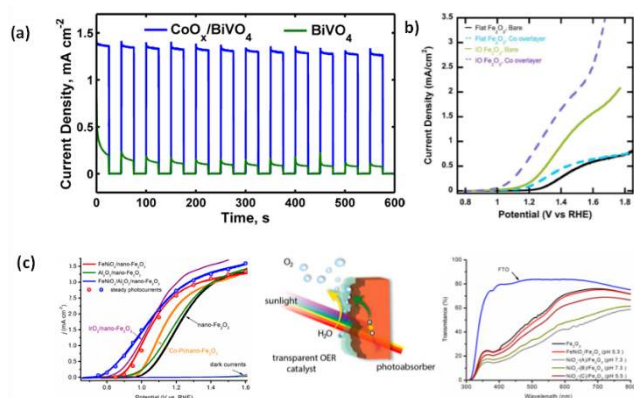

Figure 6 (a) Chopped photocurrent stability of cobalt oxide layer deposited by ALD on BiVO$_4$ photoanode at pH 13. Reproduced from Ref. [119], copyright 2013 American Chemical Society. (b) ALD-deposited submonolayer of CoO$_x$ on inverse opal hematite photoanode. Reproduced from Ref. [121], copyright 2013 American Chemical Society (c) Optically transparent FeNiO$_x$, anodically photoelectrodeposited on cauliflower and flat film hematite photoanodes, leading to a 200 mV cathodic shift of the onset potential. Reproduced from Ref. [126], copyright 2015 American Chemical Society.

10. Summary and outlook

Driven by potential technological applications, the development of metal oxide-based, non-precious OER catalysts operating in alkaline solutions has become one of the most active areas of research in chemistry and materials science. More than a decade of intense efforts in this renaissance has led to important advances in the field, including but are not limited to, (i) the identification of the universal scaling relationship between the absorbed intermediates and general descriptors, (ii) the determination of true activity trends across a wide range of metal oxides and establishment of NiFeO$_x$ as a benchmark catalyst, (iii) the in situ and operando spectroscopic characterization of catalysts, which provides previously elusive information about the catalysts, (iv) the development of novel nanomaterials which exhibit superior geometric activity. Looking ahead, two key challenges in the field can be identified: (1) The determination of active sites. The debates surrounding the active site in NiFeO$_x$ highlights the difficulty in unequivocal detection of an active site of a real-life heterogeneous catalyst even after being heavily investigated by an array of state-of-the-art experimental and computational techniques. Nevertheless, the knowledge about the active site is essential for next-step rational design and improvement of catalysts. (2) The development of catalysts with much higher intrinsic activity than the NiFeO$_x$ benchmark. It has been suggested that NiFeO$_x$ already sits on the top of the volcano plot of metal oxides in OER and is the optimal catalyst considering the scaling relationship.[58] A fine-tuning of catalyst composition might further improve the classic catalyst, as demonstrated in a recent study where W was applied to modulate CoFe oxides, providing near optimal absorption energies for intermediates.[127] To go significant beyond NiFeO$_x$, however, catalysts operate by novel reaction mechanisms which

break the scaling relationship need to be designed (or discovered).[44,45] Looking beyond academic interest, we are yet to find a successful application of the newly developed OER catalysts in a commercializable energy device. The operating conditions of real-life devices often pose stringent constraints on the choice of materials. For example, to achieve a good energy efficiency, alkaline electrolyzers operate at elevated temperatures (70-100 °C), pressures (> 10 bar), and electrolyte concentrations (concentrated KOH). The intrinsic stability of the new catalysts under these forcing conditions has not been proven. It is also challenging to maintain strong adhesion of catalyst layers to the current collectors under these conditions. Moreover, catalyst synthesis and integration should be adaptable to the manufacturing procedures of alkaline electrolyzers, while satisfying the obvious economical and scaling requirements. Intuitively, the majority of nanoparticle-type catalysts are not applicable. Changing the type of energy devices might lessen the restraint on the catalysts. For example, PEC devices will operate at much lower current densities (10 mA cm^{-2}) than electrolyzers. However, commercializable PEC devices are yet unknown and there is doubt on whether they would eventually become reality. We think a serious consideration of the suitability of a given OER catalyst in realistic energy devices is necessary in order to identify key scientific and technological road blockers. Overcoming these road blockers will then aid the realization of such energy devices, providing sustainable solutions to energy harvesting and utilization.

AUTHOR INFORMATION

Corresponding Author

*xile.hu@epfl.ch

Notes

The authors declare no competing financial interest.

ACKNOWLEDGMENT

REFERENCES

(1) Lewis, N. S.; Nocera, D. G. *Proc. Natl. Acad. Sci.* **2006**, *103*, 15729-15735.
(2) Cook, T. R.; Dogutan, D. K.; Reece, S. Y.; Surendranath, Y.; Teets, T. S.; Nocera, D. G. *Chem. Rev.* **2010**, *110*, 6474-6502.
(3) Chu, S.; Majumdar, A. *Nature* **2012**, *488*, 294-303.
(4) Suen, N. T.; Hung, S. F.; Quan, Q.; Zhang, N.; Xu, Y. J.; Chen, H. M. *Chem Soc Rev* **2017**, *46*, 337-365.
(5) Walter, M. G.; Warren, E. L.; McKone, J. R.; Boettcher, S. W.; Mi, Q.; Santori, E. A.; Lewis, N. S. *Chem. Rev.* **2010**, *110*, 6446-6473.
(6) Hunter, B. M.; Gray, H. B.; Muller, A. M. *Chem Rev* **2016**, *116*, 14120-14136.
(7) Tahir, M.; Pan, L.; Idrees, F.; Zhang, X.; Wang, L.; Zou, J.-J.; Wang, Z. L. *Nano Energy* **2017**, *37*, 136-157.
(8) Park, S.; Shao, Y.; Liu, J.; Wang, Y. *Energy Environ. Sci.* **2012**, *5*, 9331-9344.
(9) Roger, I.; Shipman, M. A.; Symes, M. D. *Nat. Rev. Chem.* **2017**, *1*, 0003.
(10) Singh, A.; Spiccia, L. *Coord. Chem. Rev.* **2013**, *257*, 2607-2622.
(11) Dau, H.; Limberg, C.; Reier, T.; Risch, M.; Roggan, S.; Strasser, P. *Chemcatchem* **2010**, *2*, 724-761.
(12) Katsounaros, I.; Cherevko, S.; Zeradjanin, A. R.; Mayrhofer, K. J. J. *Angew. Chem. Int. Ed.* **2014**, *53*, 102-121.
(13) Karkas, M. D.; Verho, O.; Johnston, E. V.; Akermark, B. *Chem Rev* **2014**, *114*, 11863-12001.
(14) Bode, H.; Dehmelt, K.; Witte, J. *Electrochim. Acta* **1966**, *11*, 1079-IN1071.

(15) Morita, M.; Iwakura, C.; Tamura, H. *Electrochim. Acta* **1977**, *22*, 325-328.

(16) El Wakkad, S.; Hickling, A. *Trans. Faraday Soc.* **1950**, *46*, 820-824.

(17) Schultze, J.; Mohr, S.; Lohrengel, M. *J. Electroanal. Chem. Interfacial Electrochem.* **1983**, *154*, 57-68.

(18) Młynarek, G.; Paszkiewicz, M.; Radniecka, A. *J. Appl. Electrochem.* **1984**, *14*, 145-149.

(19) Corrigan, D. A. *J. Electrochem. Soc.* **1987**, *134*, 377-384.

(20) Zhu, Y. P.; Guo, C.; Zheng, Y.; Qiao, S.-Z. *Acc. Chem. Res.* **2017**, *50*, 915-923.

(21) Bockris, J. O. M. *J. Chem. Phys.* **1956**, *24*, 817-827.

(22) Doyle, R.; Lyons, M. *J. Electrochem. Soc.* **2013**, *160*, H142-H154.

(23) Fang, Y.-H.; Liu, Z.-P. *ACS Catal.* **2014**, *4*, 4364-4376.

(24) Bard, A. J.; Faulkner, L. R.; Leddy, J.; Zoski, C. G. *Electrochemical methods: fundamentals and applications*; wiley New York, 1980; Vol. 2.

(25) Bockris, J. O. M.; Reddy, A. K. *Modern electrochemistry 2B: electrodics in chemistry, engineering, biology and environmental science*; Springer Science & Business Media, 1998; Vol. 2.

(26) Lyons, M. E. G.; Brandon, M. P. *J. Electroanal. Chem.* **2010**, *641*, 119-130.

(27) Meyer, R. E. *J. Electrochem. Soc.* **1960**, *107*, 847-853.

(28) Rüetschi, P.; Delahay, P. *J. Chem. Phys.* **1955**, *23*, 556-560.

(29) Trasatti, S. *J. Electroanal. Chem. Interfacial Electrochem.* **1980**, *111*, 125-131.

(30) Trasatti, S. *Electrochim. Acta* **1984**, *29*, 1503-1512.

(31) Subbaraman, R.; Tripkovic, D.; Chang, K.-C.; Strmcnik, D.; Paulikas, A. P.; Hirunsit, P.; Chan, M.; Greeley, J.; Stamenkovic, V.; Markovic, N. M. *Nat. Mater.* **2012**, *11*, 550-557.

(32) Trotochaud, L.; Young, S. L.; Ranney, J. K.; Boettcher, S. W. *J. Am. Chem. Soc.* **2014**, *136*, 6744-6753.

(33) Burke, M. S.; Zou, S.; Enman, L. J.; Kellon, J. E.; Gabor, C. A.; Pledger, E.; Boettcher, S. W. *J. Phys. Chem. Lett.* **2015**, *6*, 3737-3742.

(34) Morales-Guio, C. G.; Liardet, L.; Hu, X. *J. Am. Chem. Soc.* **2016**, *138*, 8946-8957.

(35) Bockris, J. O. M.; Otagawa, T. *J. Electrochem. Soc.* **1984**, *131*, 290-302.

(36) Liardet, L.; Hu, X. *ACS Catal.* **2018**, *8*, 644-650.

(37) Bockris, J. O. M.; Otagawa, T.; Young, V. *J. Electroanal. Chem. Interfacial Electrochem.* **1983**, *150*, 633-643.

(38) Zheng, Y.; Jiao, Y.; Zhu, Y.; Cai, Q.; Vasileff, A.; Li, L. H.; Han, Y.; Chen, Y.; Qiao, S. Z. *J Am Chem Soc* **2017**, *139*, 3336-3339.

(39) Suntivich, J.; May, K. J.; Gasteiger, H. A.; Goodenough, J. B.; Shao-Horn, Y. *Science* **2011**, *334*, 1383-1385.

(40) Grimaud, A.; May, K. J.; Carlton, C. E.; Lee, Y.-L.; Risch, M.; Hong, W. T.; Zhou, J.; Shao-Horn, Y. *Nat. Commun.* **2013**, *4*, 2439.

(41) Rossmeisl, J.; Logadottir, A.; Nørskov, J. K. *Chem. Phys.* **2005**, *319*, 178-184.

(42) Rossmeisl, J.; Qu, Z. W.; Zhu, H.; Kroes, G. J.; Nørskov, J. K. *J. Electroanal. Chem.* **2007**, *607*, 83-89.

(43) Man, I. C.; Su, H. Y.; Calle- Vallejo, F.; Hansen Heine, A.; Martínez José, I.; Inoglu Nilay, G.; Kitchin, J.; Jaramillo Thomas, F.; Nørskov Jens, K.; Rossmeisl, J. *ChemCatChem* **2011**, *3*, 1159-1165.

(44) Bendtsen Halck, N.; Petrykin, V.; Krtil, P.; Rossmeisl, J. *Phys. Chem. Chem. Phys.* **2014**, *16*, 13682-13688.

(45) Busch, M.; Halck, N. B.; Kramm, U. I.; Siahrostami, S.; Krtil, P.; Rossmeisl, J. *Nano Energy* **2016**, *29*, 126-135.

(46) Stevens, M. B.; Enman, L. J.; Batchellor, A. S.; Cosby, M. R.; Vise, A. E.; Trang, C. D. M.; Boettcher, S. W. *Chem. Mat.* **2017**, *29*, 120-140.

(47) Burke, M. S.; Kast, M. G.; Trotochaud, L.; Smith, A. M.; Boettcher, S. W. *J. Am. Chem. Soc.* **2015**, *137*, 3638-3648.

(48) Zou, S.; Burke, M. S.; Kast, M. G.; Fan, J.; Danilovic, N.; Boettcher, S. W. *Chem. Mat.* **2015**, *27*, 8011-8020.

(49) Trotochaud, L.; Ranney, J. K.; Williams, K. N.; Boettcher, S. W. *J. Am. Chem. Soc.* **2012**, *134*, 17253-17261.

(50) Trasatti, S.; Petrii, O. A. *J. Electroanal. Chem.* **1992**, *327*, 353-376.

(51) McCrory, C. C. L.; Jung, S.; Peters, J. C.; Jaramillo, T. F. *J. Am. Chem. Soc.* **2013**, *135*, 16977-16987.

(52) McCrory, C. C. L.; Jung, S.; Ferrer, I. M.; Chatman, S. M.; Peters, J. C.; Jaramillo, T. F. *J. Am. Chem. Soc.* **2015**, *137*, 4347-4357.

(53) Jung, S.; McCrory, C. C. L.; Ferrer, I. M.; Peters, J. C.; Jaramillo, T. F. *J Mater Chem A* **2016**, *4*, 3068-3076.

(54) Choi, Y. W.; Mistry, H.; Roldan Cuenya, B. *Curr. Opin.Electrochem.* **2017**, *1*, 95-103.

(55) Dionigi, F.; Strasser, P. *Adv. Energy Mater.* **2016**, *6*, 1600621.

(56) Li, J.; Guttinger, R.; More, R.; Song, F.; Wan, W.; Patzke, G. R. *Chem Soc Rev* **2017**, *46*, 6124-6147.

(57) Sasaki, K.; Wang, J. X.; Naohara, H.; Marinkovic, N.; More, K.; Inada, H.; Adzic, R. R. *Electrochim. Acta* **2010**, *55*, 2645-2652.

(58) Friebel, D.; Louie, M. W.; Bajdich, M.; Sanwald, K. E.; Cai, Y.; Wise, A. M.; Cheng, M. J.; Sokaras, D.; Weng, T. C.; Alonso-Mori, R.; Davis, R. C.; Bargar, J. R.; Norskov, J. K.; Nilsson, A.; Bell, A. T. *J Am Chem Soc* **2015**, *137*, 1305-1313.

(59) Görlin, M.; Chernev, P.; Ferreira de Araújo, J.; Reier, T.; Dresp, S.; Paul, B.; Krähnert, R.; Dau, H.; Strasser, P. *J. Am. Chem. Soc.* **2016**, *138*, 5603-5614.

(60) Li, N.; Bediako, D. K.; Hadt, R. G.; Hayes, D.; Kempa, T. J.; Cube, F. v.; Bell, D. C.; Chen, L. X.; Nocera, D. G. *Proc. Natl. Acad. Sci.* **2017**, *114*, 1486-1491.

(61) Wang, H. Y.; Hung, S. F.; Chen, H. Y.; Chan, T. S.; Chen, H. M.; Liu, B. *J Am Chem Soc* **2016**, *138*, 36-39.

(62) Corrigan, D. A.; Conell, R. S.; Fierro, C. A.; Scherson, D. A. *J. Phys. Chem.* **1987**, *91*, 5009-5011.

(63) Chen, J. Y. C.; Dang, L.; Liang, H.; Bi, W.; Gerken, J. B.; Jin, S.; Alp, E. E.; Stahl, S. S. *J. Am. Chem. Soc.* **2015**, *137*, 15090-15093.

(64) Mestl, G. *J. Mol. Catal. A* **2000**, *158*, 45-65.

(65) Yeo, B. S.; Bell, A. T. *J Am Chem Soc* **2011**, *133*, 5587-5593.

(66) Steimecke, M.; Seiffarth, G.; Bron, M. *Anal Chem* **2017**, *89*, 10679-10686.

(67) Desilvestro, J.; Corrigan, D. A.; Weaver, M. J. *J. Electrochem. Soc.* **1988**, *135*, 885-892.

(68) Trześniewski, B. J.; Diaz-Morales, O.; Vermaas, D. A.; Longo, A.; Bras, W.; Koper, M. T. M.; Smith, W. A. *J. Am. Chem. Soc.* **2015**, *137*, 15112-15121.

(69) Favaro, M.; Drisdell, W. S.; Marcus, M. A.; Gregoire, J. M.; Crumlin, E. J.; Haber, J. A.; Yano, J. *ACS Catal.* **2017**, *7*, 1248-1258.

(70) Ali-Löytty, H.; Louie, M. W.; Singh, M. R.; Li, L.; Sanchez Casalongue, H. G.; Ogasawara, H.; Crumlin, E. J.; Liu, Z.; Bell, A. T.; Nilsson, A.; Friebel, D. *J. Phys. Chem. C* **2016**, *120*, 2247-2253.

(71) Deng, J.; Nellist, M. R.; Stevens, M. B.; Dette, C.; Wang, Y.; Boettcher, S. W. *Nano Lett.* **2017**, *17*, 6922-6926.

(72) Ahn, H. S.; Bard, A. J. *J Am Chem Soc* **2016**, *138*, 313-318.

(73) Stern, L.-A.; Hu, X. *Faraday Discuss.* **2015**, *176*, 363-379.

(74) Enman, L. J.; Burke, M. S.; Batchellor, A. S.; Boettcher, S. W. *ACS Catal.* **2016**, *6*, 2416-2423.

(75) Stevens, M. B.; Trang, C. D. M.; Enman, L. J.; Deng, J.; Boettcher, S. W. *J. Am. Chem. Soc.* **2017**, *139*, 11361-11364.

(76) Görlin, M.; Ferreira de Araújo, J.; Schmies, H.; Bernsmeier, D.; Dresp, S.; Gliech, M.; Jusys, Z.; Chernev, P.; Kraehnert, R.; Dau, H.; Strasser, P. *J. Am. Chem. Soc.* **2017**, *139*, 2070-2082.

(77) Goldsmith, Z. K.; Harshan, A. K.; Gerken, J. B.; Vörös, M.; Galli, G.; Stahl, S. S.; Hammes-Schiffer, S. *Proc. Natl. Acad. Sci.* **2017**, *114*, 3050-3055.

(78) Hunter, B. M.; Thompson, N. B.; Müller, A. M.; Rossman, G. R.; Hill, M. G.; Winkler, J. R.; Gray, H. B. *Joule* **2018**, *2*, 747-763.

(79) Diaz-Morales, O.; Ferrus-Suspedra, D.; Koper, M. T. M. *Chem. Sci.* **2016**, *7*, 2639-2645.

(80) Jin, H.; Guo, C.; Liu, X.; Liu, J.; Vasileff, A.; Jiao, Y.; Zheng, Y.; Qiao, S.-Z. *Chem. Rev.* **2018**, doi: 10.1021/acs.chemrev.1027b00689.

(81) Song, F.; Hu, X. *Nat. Commun.* **2014**, *5*, 4477.

(82) Wang, L.; Lin, C.; Huang, D.; Zhang, F.; Wang, M.; Jin, J. *ACS Appl. Mater. Interfaces* **2014**, *6*, 10172-10180.

(83) Liang, H.; Meng, F.; Cabán-Acevedo, M.; Li, L.; Forticaux, A.; Xiu, L.; Wang, Z.; Jin, S. *Nano Lett.* **2015**, *15*, 1421-1427.

(84) McAteer, D.; Godwin Ian, J.; Ling, Z.; Harvey, A.; He, L.; Boland Conor, S.; Vega- Mayoral, V.; Szydłowska, B.; Rovetta Aurélie, A.; Backes, C.; Boland John, B.; Chen, X.; Lyons Michael, E. G.; Coleman Jonathan, N. *Adv. Energy Mater.* **2018**, *0*, 1702965.

(85) Zhao, Y.; Zhang, X.; Jia, X.; Waterhouse Geoffrey, I. N.; Shi, R.; Zhang, X.; Zhan, F.; Tao, Y.; Wu, L. Z.; Tung, C. H.; O'Hare, D.; Zhang, T. *Adv. Energy Mater.* **2018**, *0*, 1703585.

(86) Liu, R.; Wang, Y.; Liu, D.; Zou, Y.; Wang, S. *Adv. Mater.* **2017**, *29*, 1701546.

(87) Wang, Y.; Zhang, Y.; Liu, Z.; Xie, C.; Feng, S.; Liu, D.; Shao, M.; Wang, S. *Angew. Chem. Int. Ed.* **2017**, *56*, 5867-5871.

(88) Song, F.; Hu, X. *J. Am. Chem. Soc.* **2014**, *136*, 16481-16484.

(89) Fan, K.; Chen, H.; Ji, Y.; Huang, H.; Claesson, P. M.; Daniel, Q.; Philippe, B.; Rensmo, H.; Li, F.; Luo, Y.; Sun, L. *Nat. Commun.* **2016**, *7*, 11981.

(90) Sun, Y.; Gao, S.; Lei, F.; Liu, J.; Liang, L.; Xie, Y. *Chem. Sci.* **2014**, *5*, 3976-3982.

(91) Huang, J.; Chen, J.; Yao, T.; He, J.; Jiang, S.; Sun, Z.; Liu, Q.; Cheng, W.; Hu, F.; Jiang, Y.; Pan, Z.; Wei, S. *Angew. Chem. Int. Ed.* **2015**, *54*, 8722-8727.

(92) Bao, J.; Zhang, X.; Fan, B.; Zhang, J.; Zhou, M.; Yang, W.; Hu, X.; Wang, H.; Pan, B.; Xie, Y. *Angew. Chem. Int. Ed.* **2015**, *54*, 7399-7404.

(93) Zhao, Y.; Jia, X.; Chen, G.; Shang, L.; Waterhouse, G. I. N.; Wu, L.-Z.; Tung, C.-H.; O'Hare, D.; Zhang, T. *J. Am. Chem. Soc.* **2016**, *138*, 6517-6524.

(94) Zhao, Y.; Chang, C.; Teng, F.; Zhao, Y.; Chen, G.; Shi, R.; Waterhouse, G. I. N.; Huang, W.; Zhang, T. *Adv. Energy Mater.* **2017**, *7*, 1700005.

(95) Liang, H.; Li, L.; Meng, F.; Dang, L.; Zhuo, J.; Forticaux, A.; Wang, Z.; Jin, S. *Chem. Mat.* **2015**, *27*, 5702-5711.

(96) Xie, J.; Zhang, X.; Zhang, H.; Zhang, J.; Li, S.; Wang, R.; Pan, B.; Xie, Y. *Adv. Mater.* **2017**, *29*, 1604765.

(97) Morin, S. A.; Forticaux, A.; Bierman, M. J.; Jin, S. *Nano Lett.* **2011**, *11*, 4449-4455.

(98) Tüysüz, H.; Hwang, Y. J.; Khan, S. B.; Asiri, A. M.; Yang, P. *Nano Res.* **2012**, *6*, 47-54.

(99) Qi, J.; Zhang, W.; Xiang, R.; Liu, K.; Wang, H. Y.; Chen, M.; Han, Y.; Cao, R. *Adv. Sci.* **2015**, *2*, 1500199.

(100) Song, F.; Schenk, K.; Hu, X. *Energy Environ. Sci.* **2016**, *9*, 473-477.

(101) Ma, T. Y.; Dai, S.; Jaroniec, M.; Qiao, S. Z. *J. Am. Chem. Soc.* **2014**, *136*, 13925-13931.

(102) Jiang, J.; Zhang, A.; Li, L.; Ai, L. *J. Power Sources* **2015**, *278*, 445-451.

(103) Li, R.; Zhou, D.; Luo, J.; Xu, W.; Li, J.; Li, S.; Cheng, P.; Yuan, D. *J. Power Sources* **2017**, *341*, 250-256.

(104) Lu, X. F.; Gu, L. F.; Wang, J. W.; Wu, J. X.; Liao, P. Q.; Li, G. R. *Adv Mater* **2017**, *29*.

(105) Feng, J. X.; Xu, H.; Dong, Y. T.; Ye, S. H.; Tong, Y. X.; Li, G. R. *Angew Chem Int Ed Engl* **2016**, *55*, 3694-3698.

(106) Feng, J. X.; Ye, S. H.; Xu, H.; Tong, Y. X.; Li, G. R. *Adv Mater* **2016**, *28*, 4698-4703.

(107) Gong, M.; Li, Y. G.; Wang, H. L.; Liang, Y. Y.; Wu, J. Z.; Zhou, J. G.; Wang, J.; Regier, T.; Wei, F.; Dai, H. J. *J. Am. Chem. Soc.* **2013**, *135*, 8452-8455.

(108) Chen, S.; Duan, J. J.; Jaroniec, M.; Qiao, S. Z. *Angew. Chem. Int. Ed.* **2013**, *52*, 13567-13570.

(109) Wang, L.; Chen, H.; Daniel, Q.; Duan, L.; Philippe, B.; Yang, Y.; Rensmo, H.; Sun, L. *Adv. Energy Mater.* **2016**, *6*, 1600516.

(110) Le Formal, F.; Guijarro, N.; Bourée, W. S.; Gopakumar, A.; Prévot, M. S.; Daubry, A.; Lombardo, L.; Sornay, C.; Voit, J.; Magrez, A.; Dyson, P. J.; Sivula, K. *Energy Environ. Sci.* **2016**, *9*, 3448-3455.

(111) Hillman, A. R. *J. Solid State Electrochem.* **2011**, *15*, 1647-1660.

(112) Kim, M. S.; Hwang, T. S.; Kim, K. B. *J. Electrochem. Soc.* **1997**, *144*, 1537-1543.

(113) Frydendal, R.; Paoli, E. A.; Knudsen, B. P.; Wickman, B.; Malacrida, P.; Stephens, I. E. L.; Chorkendorff, I. *ChemElectroChem* **2014**, *1*, 2075-2081.

(114) Cherevko, S.; Geiger, S.; Kasian, O.; Kulyk, N.; Grote, J.-P.; Savan, A.; Shrestha, B. R.; Merzlikin, S.; Breitbach, B.; Ludwig, A.; Mayrhofer, K. J. J. *Catal. Today* **2016**, *262*, 170-180.

(115) Spanos, I.; Auer, A. A.; Neugebauer, S.; Deng, X.; Tüysüz, H.; Schlögl, R. *ACS Catal.* **2017**, *7*, 3768-3778.

(116) Geiger, S.; Kasian, O.; Mingers, A. M.; Nicley, S. S.; Haenen, K.; Mayrhofer, K. J. J.; Cherevko, S. *ChemSusChem* **2017**.

(117) Hu, S.; Shaner, M. R.; Beardslee, J. A.; Lichterman, M.; Brunschwig, B. S.; Lewis, N. S. *Science* **2014**, *344*, 1005-1009.

(118) Park, Y.; McDonald, K. J.; Choi, K. S. *Chem Soc Rev* **2013**, *42*, 2321-2337.

(119) Lichterman, M. F.; Shaner, M. R.; Handler, S. G.; Brunschwig, B. S.; Gray, H. B.; Lewis, N. S.; Spurgeon, J. M. *J. Phys. Chem. Lett.* **2013**, *4*, 4188-4191.

(120) Shen, S.; Lindley, S. A.; Chen, X.; Zhang, J. Z. *Energy Environ. Sci.* **2016**, *9*, 2744-2775.

(121) Riha, S. C.; Klahr, B. M.; Tyo, E. C.; Seifert, S.; Vajda, S.; Pellin, M. J.; Hamann, T. W.; Martinson, A. B. F. *Acs Nano* **2013**, *7*, 2396-2405.

(122) Du, C.; Yang, X.; Mayer, M. T.; Hoyt, H.; Xie, J.; McMahon, G.; Bischoping, G.; Wang, D. *Angew. Chem. Int. Ed.* **2013**, *52*, 12692-12695.

(123) Smith, R. D. L.; Prevot, M. S.; Fagan, R. D.; Zhang, Z. P.; Sedach, P. A.; Siu, M. K. J.; Trudel, S.; Berlinguette, C. P. *Science* **2013**, *340*, 60-63.

(124) Trotochaud, L.; Mills, T. J.; Boettcher, S. W. *J. Phys. Chem. Lett.* **2013**, *4*, 931-935.

(125) McKone, J. R.; Lewis, N. S.; Gray, H. B. *Chem. Mat.* **2014**, *26*, 407-414.

(126) Morales-Guio, C. G.; Mayer, M. T.; Yella, A.; Tilley, S. D.; Grätzel, M.; Hu, X. *J. Am. Chem. Soc.* **2015**, *137*, 9927-9936.

(127) Zhang, B.; Zheng, X.; Voznyy, O.; Comin, R.; Bajdich, M.; García-Melchor, M.; Han, L.; Xu, J.; Liu, M.; Zheng, L. *Science* **2016**, *352*, 333-337.
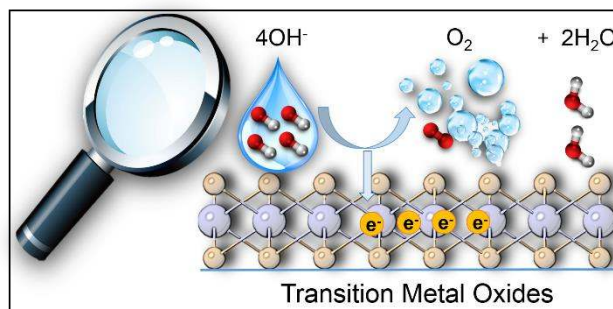
Insert Table of Contents artwork here